Ge/Si nanowire mesoscopic Josephson junctions

JIE XIANG[1], A. VIDAN[2]*, M. TINKHAM[2,3], R. M. WESTERVELT[2,3]† AND CHARLES M. LIEBER[1,2]†

[1]Department of Chemistry and Chemical Biology, Harvard University, Cambridge, Massachusetts 02138, USA
[2]Division of Engineering and Applied Sciences, Harvard University, Cambridge, Massachusetts 02138, USA
[3]Department of Physics, Harvard University, Cambridge, Massachusetts 02138, USA
*Present address: MIT Lincoln Laboratory, Lexington, Massachusetts 02420, USA
†e-mail: westervelt@deas.harvard.edu, cml@cmliris.harvard.edu

Published online: 5 December 2006; doi:10.1038/nnano.2006.140

The controlled growth of nanowires (NWs) with dimensions comparable to the Fermi wavelengths of the charge carriers allows fundamental investigations of quantum confinement phenomena. Here, we present studies of proximity-induced superconductivity in undoped Ge/Si core/shell NW heterostructures contacted by superconducting leads. By using a top gate electrode to modulate the carrier density in the NW, the critical supercurrent can be tuned from zero to greater than 100 nA. Furthermore, discrete subbands form in the NW due to confinement in the radial direction, which results in stepwise increases in the critical current as a function of gate voltage. Transport measurements on these superconductor–NW–superconductor devices reveal high-order ($n = 25$) resonant multiple Andreev reflections, indicating that the NW channel is smooth and the charge transport is highly coherent. The ability to create and control coherent superconducting ordered states in semiconductor–superconductor hybrid nanostructures allows for new opportunities in the study of fundamental low-dimensional superconductivity.

When two superconductors are weakly connected, for example in a superconductor–normal-conductor–superconductor (S–N–S) structure, a dissipationless supercurrent can flow through the junction as a result of the Josephson effect, which originates from the fixed phase differences between the electron wavefunctions in the two superconductors across the normal conductor[1,2]. This type of device is known as a Josephson junction, with the maximum magnitude of the supercurrent flowing across the junction defined as the Josephson critical current, I_c. In the clean limit of a conventional metallic junction[1], the product of I_c with normal state resistance R_n is a constant proportional to the Bardeen-Cooper-Schrieffer (BCS) energy gap parameter Δ; that is, $I_c R_n = \pi\Delta/e$, where e is the fundamental charge of an electron. The $I_c R_n$ product is independent of sample geometry, because the same junction-geometry-dependent terms cancel each other out in I_c and R_n (refs 1 and 2). Interestingly, a new mesoscopic regime emerges when the width w of the normal conductor shrinks to become comparable to the carrier Fermi wavelength λ_F, and its normal-state conductance becomes quantized in multiples of $2e^2/h$, regardless of the exact length of the constriction due to the effect of one-dimensional (1D) quantum confinement[3]. It has been predicted[4] that the universal product $I_c R_n = \pi\Delta/e$ also holds for short Josephson junctions with discrete transverse modes, where each of the N modes forms an independent Andreev bound level and contributes the same amount to the total supercurrent[4,5], thus $I_c = Ne\Delta/\hbar$, although such a regime has not been reached experimentally[6,7]. In most previous investigations of S–N–S structures, conventional metals have been used to form the junctions. In these junctions, the $w \approx \lambda_F$ regime is difficult to achieve as it would require a stable and controllable junction only a few atoms wide[8]. This limitation can be overcome using semiconductors, because of their low carrier density and correspondingly large Fermi wavelength. Previous experimental studies with Nb-contacted quantum point contacts (QPCs) in a two-dimensional electron gas[6,7] reported steps in I_c, although these were two orders of magnitude smaller than $e\Delta/\hbar$ and were dependent on the sample geometry owing to the large sample size (with length $L \gg \xi_0$, where ξ_0 is the coherence length characteristic of the superconductor).

The nanoscale dimensions and tunability of the carrier density with applied gate voltage in chemically synthesized semiconductor NWs make them promising platforms to carry out such studies. Indeed, recent advances in the chemical growth and physical understanding of NWs (refs 9 and 10) have enabled the study of a broad range of transport phenomena associated with quantum confinement effects and reduced dimensionality, such as single-charge tunnelling[11–13] and coherent ballistic transport with controlled access of multiple 1D subbands[14], and have contributed to high-performance field-effect transistors[15]. Furthermore, the recent pioneering work by Kouwenhoven and co-workers has demonstrated supercurrents in n-type InAs NWs (ref. 16) and has enabled the study of supercurrents coupled with Coulomb blockade phenomena in quantum dots[17], although the relatively large diameters and small mean free paths in these NWs suggest that carrier transport was in the bulk diffusive regime. On the other hand, the low dimensional carrier gas in epitaxial Ge/Si core/shell NW heterostructures[14,15] (Fig. 1a) has a high mobility, low scattering, and it is possible to reproducibly make ohmic contacts. These characteristics, along with the ability to tune conduction down to the first few 1D modes in the quantum-confined Ge channel make Ge/Si NWs ideal for the study of the interplay between 1D quantum confinement and

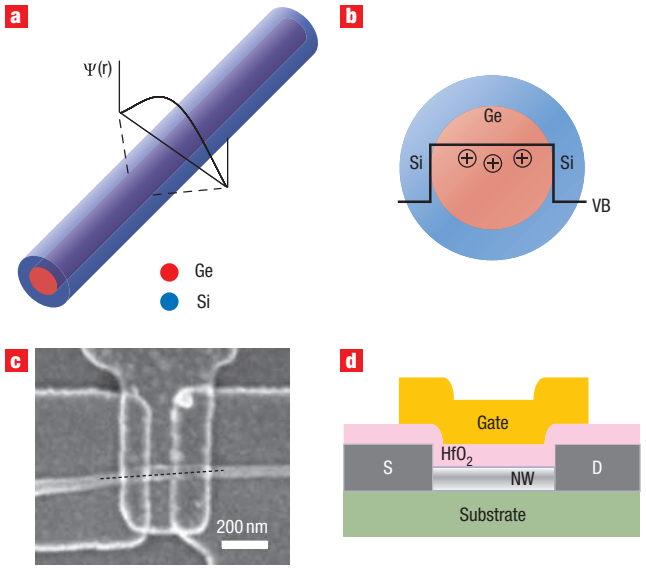

Figure 1 Schematic diagram and device image of a Ge/Si nanowire device. **a**, Schematic of a Ge/Si core/shell nanowire heterostructure. Also shown is the radial wavefunction $\Psi(r)$ for the lowest 1D sub-band in a cylindrical quantum wire, where the Fermi wavelength is comparable to twice the channel diameter w. **b**, Cross-sectional diagram showing the hole gas in the Ge quantum well confined by the epitaxial Si shell, where VB is the valence band energy. **c**, Scanning electron microscopy image of a representative top-gated device. The dashed line highlights the position of the nanowire. **d**, Cross-sectional schematic of the device along the dashed line in **c** showing the Al source(S)/drain(D) contact electrodes, HfO_2 dielectric and Cr/Au top gate.

superconductivity. In this paper we use superconducting aluminium as contacts to individual Ge/Si NWs in order to investigate this novel regime (Fig. 1c, d). Measurements on a single S–NW–S device revealed a tunable critical supercurrent I_c of greater than 100 nA. At finite bias voltage, the device exhibited resonant multiple Andreev reflection peaks in differential conductance up to order 25, indicating that the NW channel is smooth and transport is highly coherent[5,18,19]. Finally, we found that I_c exhibits steps at gate voltage values corresponding to the normal state conductance plateaus due to radial carrier confinement.

RESULTS AND DISCUSSION

FABRICATION OF Ge/Si NW DEVICES

The Ge/Si core/shell NWs were grown using a two-step chemical vapour deposition process, and have a Ge core diameter of ~15 nm and Si shell thickness of ~1.5–2 nm (refs 15 and 20). As shown in previous studies[14,15], the epitaxial Si shell provides a clean confinement potential for the hole gas in the Ge core because of the ~500 mV valence band differences between the two semiconductors (Fig. 1b). After growth, Al contacts were fabricated on the NW devices by electron-beam lithography and thermal evaporation with a typical contact separation length (which defines the length L of the Josephson junction) of 100–150 nm (see Methods). A top-gated structure with high-κ dielectric[15] was used to control the Fermi level and hole carrier density inside the NW (Fig. 1c, d). The contacts were not intentionally annealed, although we believe Fermi-level pinning due to interfacial states and diffusion of aluminium during the fabrication process are responsible for the ohmic contacts to the Ge hole gas at low temperature.

NORMAL-STATE CHARACTERISTICS

Figure 2a shows the differential conductance, dI/dV, as a function of source–drain voltage V in a 150-nm-long NW. The measurement was performed at 10 K so that the aluminium leads were non-superconducting. The different curves correspond to different values of the top gate voltage V_g. In the linear regime (around $V = 0$), dark bunching regions, where several curves at different V_g overlap, are observed and are spaced vertically by approximately $2e^2/h$. This is consistent with quantized conductance plateaus for individual spin degenerate 1D sub-bands[3], because V_g has little effect on dI/dV in the plateau regions. The irregularities in the vertical locations and the spread of these bunching regions correspond to fluctuations in the plateau height and shape and can be attributed to finite reflectivity at both contacts[21], or to scattering of carrier waves with potential irregularities similar to those observed in a QPC (ref. 22). A further indication of the presence of the conductance plateaus can be seen in the nonlinear transport regime, around $V \approx \pm 20$ mV. At these higher bias voltage, the plateaus (bunching) at zero bias evolve into 'half' plateaus when the source and drain chemical potentials cross different subbands, as reported previously in QPCs and 1D quantum wires[23,24]. From the crossing point where half plateaus form in Fig. 2a, we are able to obtain a sub-band spacing energy δE of ~20–30 meV, consistent with an estimation from a 15-nm-diameter cylindrical confinement potential[14].

JOSEPHSON SUPERCURRENTS

The device was cooled in a dilution refrigerator with base temperature of 60 mK, far below the superconducting transition temperature T_c of the Al contacts ($T_c = 1.6$ K), to enable studies of the superconducting proximity effect. A key criterion for the observation of supercurrents in an S–N–S junction is $E_J \gg k_B T$, where E_J is the Josephson junction energy[1], and k_B is the Boltzmann constant. Therefore, it is important to keep the device thermally coupled to a low base temperature, as well as to reduce radiation noise fed down from the electronic circuitry, preventing electronic heating of the sample. We incorporated several stages of noise filters into the measurement system in order to keep the effective electronic temperature of the sample device close to the temperature of the mixing chamber in the dilution refrigerator (see Methods and Supplementary Information, Fig. S1). The device was measured in a four-probe geometry by wire-bonding a pair of wires onto each of the two Al contact pads (see Supplementary Information, Figs. S1 and S2).

Figure 2b shows a typical voltage–current (V–I) characteristic of a Ge/Si nanowire device with $L = 100$ nm, measured in a four-probe current bias configuration. The data exhibit clear dissipationless supercurrent with zero voltage drop and effectively zero resistance as the applied current bias is swept from zero up to an I_c of 113 nA; that is, the Ge/Si nanowire becomes superconducting with the formation of Cooper pairs inside the Ge channel due to penetration of the BCS wavefunction from the Al electrodes. Beyond I_c, the $V(I)$ curve abruptly switches to normal-state dissipative conduction with a finite slope (black arrow). We note, however, that the observed I_c may only represent a fraction of the junction's actual Josephson critical current I_{c0} because of premature switching caused by thermal activation[1]. When the current bias was swept down (red arrow), $V(I)$ switched back to the dissipationless state at a return current I_r smaller than I_c. This hysteretic behaviour may be the result of phase instability due to dissipative coupling to the environment

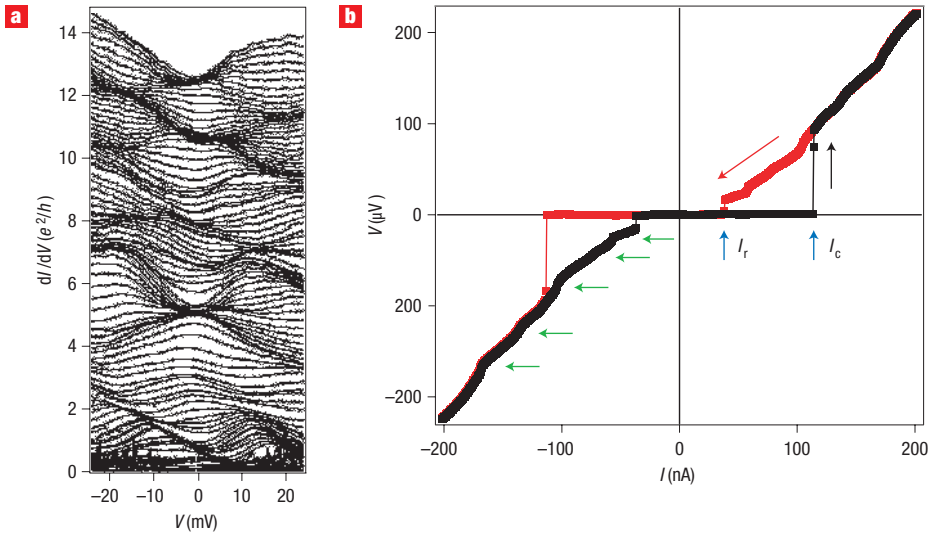

Figure 2 Transport characteristics of Ge/Si nanowire above and below the superconducting transition temperature. a, (d*I*/d*V*)–*V* plots recorded at $V_g = 0.8$ to -3.5 V from bottom up in 50-mV steps with no offset applied ($T = 10$ K). An offset resistance of 5 kΩ was subtracted from the data to account for the fixed series resistance in this two-probe measurement as well as effects arising from the finite contact resistance and scattering with impurity potentials inside the nanowire. Coulomb charging effects were not observed at temperatures down to at least 5 K for all gate voltages. **b**, Four-probe *V*–*I* data measured for a Ge/Si nanowire at $V_g = -3.5$ V at the dilution refrigerator base temperature of 60 mK. Black and red curves correspond to different current sweeping directions as indicated by arrows. The horizontal green arrows point to the kink structures due to multiple Andreev reflections. Blue vertical arrows point to the positions of the critical current, I_c and the return current, I_r.

in an underdamped Josephson junction[1], or may simply be due to a heating effect[25]. Most importantly, the I_c of 113 nA and the supercurrent density of 6.4×10^4 A cm^{-2} are the highest observed in individual semiconductor nanowires[16], indicating the high contact quality of the Ge/Si nanowires as well as the effectiveness of the noise filtering system.

MULTIPLE ANDREEV REFLECTIONS

A series of kink-like features are observed in the normal branch of the $V-I$ curve of Fig. 2b (green arrows). We attribute these features to multiple Andreev reflections (MARs) (refs 5 and 19). In the Andreev reflection process, an incident electron at the N–S interface becomes a Cooper pair in the condensate of the superconducting leads, resulting in a hole being coherently reflected into the normal conductor, and vice versa. In a clean conductor, this process provides the microscopic mechanism responsible for the superconducting proximity effect[5]. MARs allow for 'Andreev channels' to open up in the S–N–S junction at bias voltages below the superconducting energy gap 2Δ. These Andreev channels arise from a progressive increase of the incident carrier energy as the carrier reflects between the two interfaces. Each time the electron (or hole) travels across the junction, it picks up an energy eV. When the sum of the energy gain equals 2Δ of the contact leads, a resonant enhancement in the differential conductance results, which in turn appears as kinks in the $V-I$ curve[19].

Figure 3a shows a plot of d*I*/d*V* as a function of the *V* measured using a four-probe lock-in method (see Methods and Supplementary Information, Fig. S2), highlighting the kink features seen in the $V-I$ data. In this plot, a family of peak features is observed, symmetrically around $V = 0$. The peak at $V = 0$ has a height greater than 1×10^4 e^2/h, and corresponds to 'infinite conductivity' when the Ge/Si NW is superconducting. The actual peak height is limited by several factors, including the applied a.c. excitation voltage, the data acquisition rate, as well as the resolution of the voltage amplifiers. The peaks at finite source–drain voltage correspond to the subharmonic energy-gap structure caused by MARs, with peak positions given by $eV_n = 2\Delta/n$ ($n = 1, 2, 3, \ldots$), as expected[19]. From a fit of the MARs peak positions (Fig. 3b) we can determine that $\Delta = 235$ μeV and find that the observed peaks correspond to $n = 1$, 2, 3, 4, 5, 9, 13 and 25. Using the BCS relation $\Delta = 1.76\, k_B T_C$ (ref. 1), the measured energy gap $\Delta = 235$ μeV corresponds to $T_c = 1.6$ K for the Al leads. The arrows and dashed lines in Fig. 3a mark the calculated peak positions for different values of n and demonstrate the excellent fit of the observed data with theory. We note that the position of the $n = 1$ peak at high bias does not agree with this energy-gap value, likely due to heating of the junction at high bias voltages[26] that would reduce Δ. These observed subharmonic peaks are well reproducible and independent of sweep direction. Within our measurement resolution as well as the limits of thermal broadening, we did not observe any peak feature corresponding to $n \approx 6-8$. Besides these missing peaks, it is also quite interesting to see non-consecutive high-order reflections ($n = 9$, 13, 25) with larger amplitude than the $n = 5$ peak. An exact explanation of these observations is not yet clear. However, we note that our preliminary study of the magnetic-field-dependence of these subharmonic peak positions shows a systematic shift to lower energy that is consistent with the decrease in 2Δ with increasing field, and is evidence that all the observed peaks originate from resonant Andreev reflections.

We are not aware of such a clear signature of MARs being reported previously. As a point of reference, the $n = 25$ subharmonic peak requires that the charge carrier traverse the channel 25 times without being backscattered inside the channel. Moreover, measurements of d*I*/d*V* as a function of both *V* and top gate voltage V_g (Fig. 3c) show that Andreev peak positions of

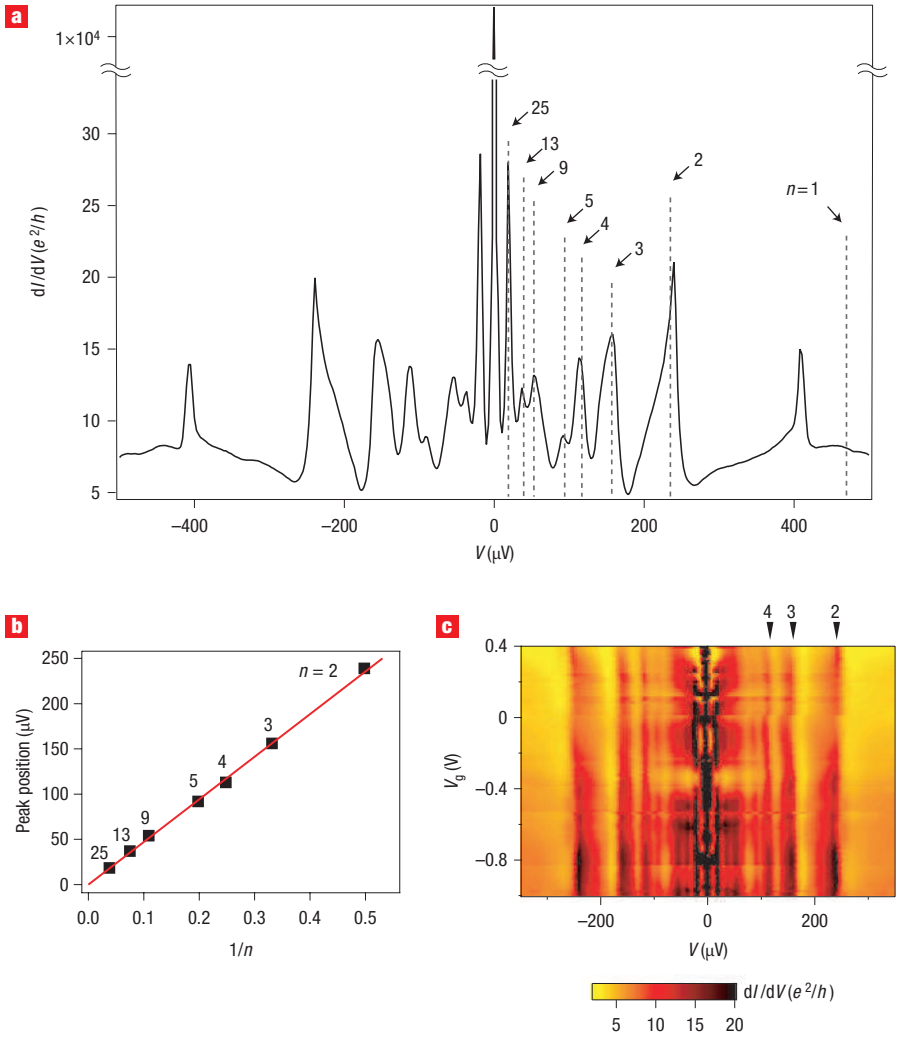

Figure 3 Multiple Andreev reflections in the Ge/Si nanowire device. a, The d*I*/d*V* versus *V* data were taken in a four-probe geometry (see Supplementary Information, Fig. S2) at $V_g = -900$ mV. Arrows and dashed lines mark the theoretical MAR peak positions at $V_n = 2\Delta/ne$ with values of *n* indicated. **b**, Plot of the MAR peak position versus the inverse index $1/n$. The red line is a linear fit of all the points (except $n = 1$) through the origin, and the slope is proportional to the gap energy. **c**, (d*I*/d*V*)–V–V_g plot showing the MAR features at different gate voltages. The arrows and numbers at the top indicate the corresponding *n*th order MAR features.

order $n = 2$ or higher remain constant with V_g. This contrasts with the complicated shifts and oscillatory behaviour of MAR peaks around a resonant level in a quantum dot[27,28], and suggests the absence of such localized states in our NWs. The higher order MARs further indicate that the contacts are quite transparent. The contact transparency can be estimated from the BTK theory of the effect of interfacial barriers[29,30] using the $V-I$ curve for $V > 2\Delta/e$ (see Methods and Supplementary Information, Fig. S3). This yields a value of 80%, which is among the highest observed in superconductor–semiconductor interfaces[16,17]. This high contact transparency is maintained for different values of the gate voltage in all of the devices studied, and demonstrates that reproducible, transparent contacts can be formed using band-structure-engineered NW heterostructures.

In addition, we note that device yield is quite good. We have successfully measured 18 devices with similar dimensions in a ^{3}He cryostat with base temperature of 300 mK, of which 11 with normal on-state resistance $R_{on} < 20\,k\Omega$ were found to exhibit pronounced enhancement of zero-bias conductance and subharmonic peak structures due to the superconducting proximity effect and MAR. The remaining devices (with $R_{on} > 20\,k\Omega$) showed Coulomb blockade oscillations, presumably due to nonideal contact interfaces. The relatively high base temperature and lack of noise filtering system in this ^{3}He cryostat have precluded detailed studies of the Josephson supercurrents. However, two devices were mounted in the dilution refrigerator, and in both cases clear dissipationless supercurrents were observed, one of which is presented here. In the second device, we observed 6–8 peaks on each side of the voltage bias axis. Analysis of these data suggests missing intermediate-order MAR peaks similar to the data shown in Fig. 3a, although, because the sample was measured in a two-probe configuration with lower resolution, we do not believe it is reasonable to make an unambiguous designation of peak orders.

CORRELATION BETWEEN I_c AND NORMAL-STATE CONDUCTANCE PLATEAUS

The top-gated device structure allows us to substantially vary the carrier density in the Ge/Si NW heterostructures[14,15]. $V-I$ measurements made as a function of V_g (Fig. 4a) demonstrate

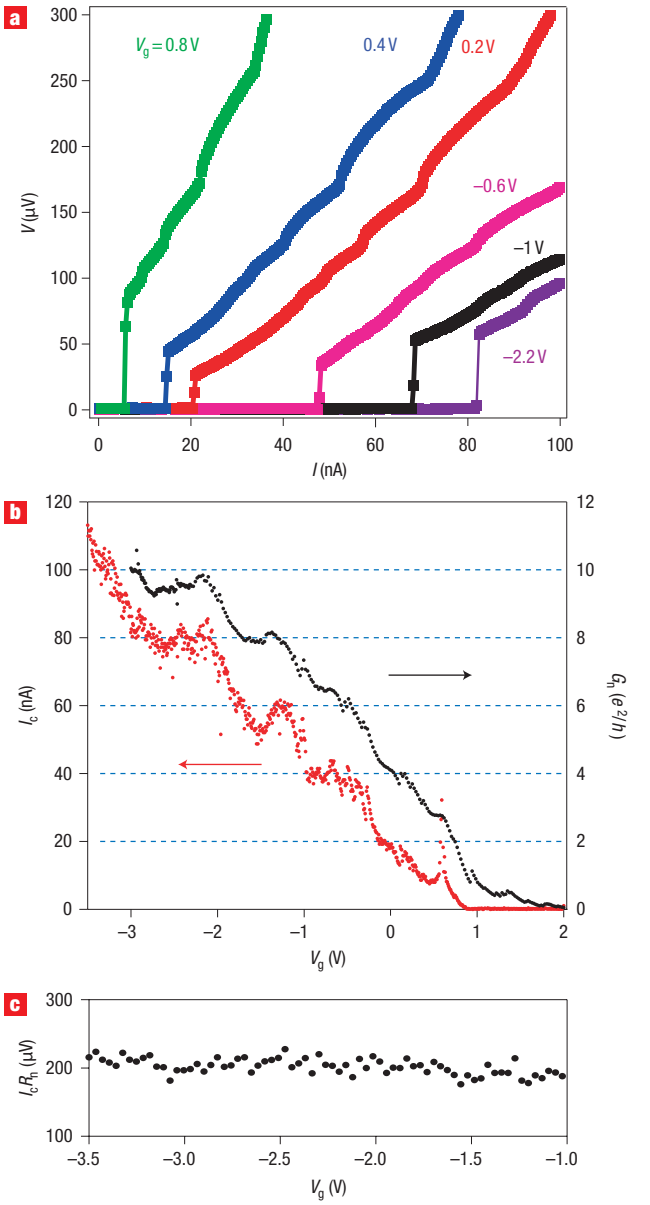

Figure 4 Gate-voltage dependence of critical current and normal conductance. a, *V*–*I* curves for the same Ge/Si nanowire device measured at different gate voltages. All curves were taken while sweeping the current from zero to 100 nA. **b**, Normal-state d*I*/d*V* versus V_g curve (black) and I_c versus V_g (red). The normal-state conductance was measured in a four-probe geometry at zero bias ($V = 0$) with applied magnetic field $H = 250$ mT. A series resistance of $R_s = 200\ \Omega$ has been subtracted. I_c is extracted from individual *V*–*I* measurements as the onset of voltage switching in the direction of the black arrow in Fig. 2b. **c**, Product of I_c and R_n versus gate voltage, where R_n is extracted from the slope of the individual *V*–*I* curve at voltages larger than $2\Delta/e$, or 470 μV.

that I_c decreases with increasing V_g from −2.2 to 0.8 V; that is, I_c decreases as the carrier density is reduced. These results suggest that the extent of the superconductive coupling can be tuned with the change of the carrier density inside the semiconductor NW, which thus provides an additional experimental knob that is not available in conventional S–N–S junctions using metallic weak links[2].

We have analysed further the V_g dependence of I_c by comparing the measured I_c and normal-state conductance G_n as a function of V_g (Fig. 4b). The normal-state conductance was obtained at zero bias while applying a 250 mT magnetic field, which completely suppresses superconductivity in the aluminium electrodes. The zero-bias $G_n \equiv dI/dV$ (Fig. 4b, black curve) shows plateau features at conductance values of multiples of $2e^2/h$, similar to those observed at temperatures above T_c (Fig. 2a), indicative of transport through individual 1D sub-bands in the germanium channel. The critical current I_c (red) also shows an increase as V_g is reduced, and the NW remains superconducting after I_c has been 'turned on' at around $V_g = 900$ mV. This behaviour contrasts with previous observations in carbon nanotube S–N–S junctions, where I_c showed oscillatory on–off behaviour due to interaction of the BCS states with resonant levels in the nanotube[27]. Significantly, our measured I_c increases stepwise with a step height of $\delta I_c \sim 20$ nA, strongly suggestive of quantization in superconducting critical current in our Ge/Si NW heterostructure.

The correlation between the plateau structures at quantized values in the $I_c - V_g$ and $G_n - V_g$ curves can in fact be confirmed by plotting the ratio of I_c and G_n, or the I_cR_n product against V_g as shown in Fig. 4c, where $R_n \equiv 1/G_n$ is the normal-state resistance. The I_cR_n product is essentially a constant at around 200 μV, over a wide range of gate voltages, indicating that the steps in I_c occur when individual sub-bands are populated in the NW. Furthermore, the ratio of the measured I_cR_n with Δ/e reaches 85% and is substantially higher than previous studies using InAs NWs and carbon nanotubes, which yield $I_cR_n/(\Delta/e)$ ratios of only 15–47% (refs 16 and 27).

These results can be compared with theoretical predictions. In the clean limit (mean free path $l > \xi_0$), the Ge/Si nanowire coherence length is $\xi_0 = \hbar v_F/\pi\Delta = 140$ nm, where the Fermi velocity $v_F = 1.5\times10^5$ m s^{-1} is estimated by assuming a Fermi energy of 20 meV on the first sub-band, and ξ_0 will increase for higher energy sub-bands. The 1D Ge/Si NW channels in our measurements thus fall into the regime $L \ll \xi_0$ where theory[4] predicts that $I_cR_n = \pi\Delta/e$ and that the critical current increases in steps of $\delta I_c = e\Delta/\hbar$. The measured $I_cR_n = 200$ μV differs from $\pi\Delta/e = 738$ μV by a factor of ~3.6. This discrepancy can be explained by premature switching due to thermal activation in a capacitively and resistively shunted junction[1], which would lead to a measured I_c smaller than the actual Josephson critical current I_{c0}. Consistent with this explanation we also observe a value of $\delta I_c = 20$ nA that is a factor of three lower than the predicted value $\delta I_c = e\Delta/\hbar = 57$ nA. Note that the finite contact transparency, as well as the limited L/ξ_0 value, may also contribute to the observed reduction factor in δI_c and I_cR_n. We expect that optimization of the junction geometry by, for example, using a shorter junction, minimizing the stray capacitance from the contact leads and improving the measurement to further reduce the sample effective temperature, will yield values of I_c closer to the universal predictions. Despite these limitations, the work presented here is the first study of the superconducting proximity effect coupled with discrete 1D modes in the $L \ll \xi_0$ regime, whereas previous efforts in QPCs with $L \gg \xi_0$ achieved δI_c values two orders of magnitude smaller (compared with a factor of 3–4 in our work) than the universal value of $e\Delta/\hbar$ (refs 6 and 7).

In summary, we have presented studies of mesoscopic Josephson junctions using Ge/Si NW heterostructures that demonstrate tunable dissipationless supercurrents as well as clear signatures of multiple Andreev reflections. Significantly, by tuning the carrier density to populate discrete 1D modes we show a distinct correlation between the quantized normal-state conductance and the steps in the critical current. The smooth,

scattering-free 1D confinement potential in the Ge/Si nanowire channel, along with the local top-gate device structure, will allow the use of Josephson junctions as tunable superconducting field-effect transistors and unique quantum interference devices. More generally, the ability to couple low-dimensional systems with superconducting phenomena opens new opportunities in this interesting mesoscopic regime.

METHODS

FABRICATION OF Ge/Si NW DEVICES

Epitaxial core–shell Ge/Si NWs with an average core diameter of 14.6 nm and Si shell thickness of 1.7 nm, and <110> core growth direction were prepared as described previously[14,15,20]. Al source/drain contact electrodes (30 nm thickness) were defined by electron-beam lithography and deposited by thermal evaporation. The nanowires and source/drain electrodes were then covered with a 10-nm HfO_2 high dielectric constant layer (80 cycles using atomic layer deposition)[15], and then electron-beam lithography was used to define the top gate, followed by thermal evaporation of Cr/Au (5/50 nm).

LOW-NOISE MEASUREMENT SETUP

We used three stages of filtering on all the electrical leads. An illustration of the experimental setup is shown in the Supplementary Information, Fig. S1. At room temperature, π filters (Spectrum Control) are placed on each electrical lead before they enter the cryostat. The π filters are mounted inside a Pomona box (Pomona Electronics) through a RF-tight copper divider. The copper divider separates the 'in' section from the 'out' section to further shield the outgoing signal from radiation. Above 1 MHz, the measured attenuation of these π filters is 80 dB. A second stage of filtering is provided by 10-kΩ metal film resistors embedded in a copper chuck. The copper chuck is thermally anchored to the mixing chamber. The 10-kΩ metal film resistors, along with the cable inductance and capacitance, serve as cold low-pass RLC filters with an estimated noise cut-off frequency of 10 kHz. The final stage of filtering of the leads, effective for frequencies above 1 GHz, is provided by a copper powder filter that is integrated on the cold finger of the dilution refrigerator. The area between the inner and outer tubes of the cold finger is filled with a mixture of surface-oxidized copper powder and epoxy (Stycast #1266, Emerson and Cuming), and six feet of wires were coiled inside this cavity before being connected to the sample. Finally, the ^{3}He/^{4}He dilution refrigerator and the measurement electronics sit inside a sealed shielded room. The data acquisition computer is placed outside the shielded room, and communicates with the measurement electronics via optical fibres.

Four-probe measurements, as depicted in Fig. S2 (see Supplementary Information), were used to obtain voltage-bias measurements of dI/dV. The four probes were formed by wire-bonding a pair of wires onto each aluminium contact pad.

ESTIMATION OF CONTACT TRANSPARENCY USING BTK THEORY

At voltages larger than the BCS gap 2Δ, transport can occur via the excited carriers in the leads and is no longer superconducting in nature. This can be seen in Fig. S3 (see Supplementary Information), where a fit to the V–I curve at the normal state above 2Δ extrapolates to a finite excess current I_{exc} (red solid line) and does not go through the origin. This is a clear manifestation of the conductance enhancement below $V = 2\Delta$ due to the superconducting proximity effect. The slope of the line yields the normal-state resistance R_n. We analysed I_{exc} and R_n under the framework of the standard BTK theory[29,30]. In this particular case, $I_{exc} = 78$ nA, $R_n = 3.5$ kΩ. Using $\Delta = 235$ μeV we obtain $eI_{exc}R_n/\Delta = 1.16$, which corresponds to a contact transparency of 80%. Similar values for the contact transparency are obtained at different gate voltages. We note that this calculation of contact transparency is a conservative estimate as it does not include the reduction of BCS gap at high bias, as manifested by the shift of the $n = 1$ MAR peak. For example, if the gap energy is reduced to 85% of the value at lowest temperature, in our case the $eI_{exc}R_n/\Delta$ would increase from 1.16 to 1.36, and the obtained contact transparency would increase to 85% from 80%.

Received 29 August 2006; accepted 1 November 2006; published 5 December 2006.

References

1. Tinkham, M. *Introduction to Superconductivity* (Dover, New York, 1996).
2. Likharev, K. K. Superconducting weak links. *Rev. Mod. Phys.* **51,** 101–159 (1979).
3. Van Wees, B. J. *et al.* Quantized conductance of point contacts in a two-dimensional electron-gas. *Phys. Rev. Lett.* **60,** 848–850 (1988).
4. Beenakker, C. W. J. & Van Houten, H. Josephson current through a superconducting quantum point contact shorter than the coherence length. *Phys. Rev. Lett.* **66,** 3056–3059 (1991).
5. Klapwijk, T. M. Proximity effect from an Andreev perspective. *J. Supercond.* **17,** 593–611 (2004).
6. Takayanagi, H., Akazaki, T. & Nitta, J. Observation of maximum supercurrent quantization in a superconducting quantum point-contact. *Phys. Rev. Lett.* **75,** 3533–3536 (1995).
7. Bauch, T. *et al.* Correlated quantization of supercurrent and conductance in a superconducting quantum point contact. *Phys. Rev. B* **71,** 174502 (2005).
8. Muller, C. J., Vanruitenbeek, J. M. & DeJongh, L. J. Conductance and supercurrent discontinuities in atomic-scale metallic constrictions of variable width. *Phys. Rev. Lett.* **69,** 140–143 (1992).
9. Lieber, C. M. Nanoscale science and technology: Building a big future from small things. *MRS Bulletin* **28,** 486–491 (2003).
10. Samuelson, L. Self-forming nanoscale devices. *Mater. Today* **6,** 22–31 (2003).
11. Zhong, Z. H., Fang, Y., Lu, W. & Lieber, C. M. Coherent single charge transport in molecular-scale silicon nanowires. *Nano Lett.* **5,** 1143–1146 (2005).
12. De Franceschi, S. *et al.* Single-electron tunneling in InP nanowires. *Appl. Phys. Lett.* **83,** 344–346 (2003).
13. Bjork, M. T. *et al.* Few-electron quantum dots in nanowires. *Nano Lett.* **4,** 1621–1625 (2004).
14. Lu, W., Xiang, J., Timko, B. P., Wu, Y. & Lieber, C. M. One-dimensional hole gas in germanium/silicon nanowire heterostructures. *Proc. Natl Acad. Sci. USA* **102,** 10046–10051 (2005).
15. Xiang, J. *et al.* Ge/Si nanowire heterostructures as high-performance field-effect transistors. *Nature* **441,** 489–493 (2006).
16. Doh, Y. J. *et al.* Tunable supercurrent through semiconductor nanowires. *Science* **309,** 272–275 (2005).
17. Van Dam, J. A., Nazarov, Y. V., Bakkers, E. P. A. M., De Franceschi, S. & Kouwenhoven, L. P. Supercurrent reversal in quantum dots. *Nature* **442,** 667–670 (2006).
18. Andreev, A. F. The thermal conductivity of the intermediate state in superconductors. *Sov. Phys. JETP* **19,** 1228–1231 (1964).
19. Octavio, M., Tinkham, M., Blonder, G. E. & Klapwijk, T. M. Subharmonic energy-gap structure in superconducting constrictions. *Phys. Rev. B* **27,** 6739–6746 (1983).
20. Lauhon, L. J., Gudiksen, M. S., Wang, C. L. & Lieber, C. M. Epitaxial core–shell and core–multishell nanowire heterostructures. *Nature* **420,** 57–61 (2002).
21. Van Wees, B. J. *et al.* Quantum ballistic and adiabatic electron-transport studied with quantum point contacts. *Phys. Rev. B* **43,** 12431–12453 (1991).
22. Topinka, M. A. *et al.* Imaging coherent electron flow from a quantum point contact. *Science* **289,** 2323–2326 (2000).
23. Cronenwett, S. M. *et al.* Low-temperature fate of the 0.7 structure in a point contact: A Kondo-like correlated state in an open system. *Phys. Rev. Lett.* **88,** 226805 (2002).
24. Kristensen, A. *et al.* Bias and temperature dependence of the 0.7 conductance anomaly in quantum point contacts. *Phys. Rev. B* **62,** 10950–10957 (2000).
25. Tinkham, M., Free, J. U., Lau, C. N. & Markovic, N. Hysteretic I–V curves of superconducting nanowires. *Phys. Rev. B* **68,** 134515 (2003).
26. Octavio, M., Skocpol, W. J. & Tinkham, M. Improved performance of tin variable-thickness superconducting microbridges. *IEEE Trans Magn.* **13,** 739–742 (1977).
27. Jarillo-Herrero, P., van Dam, J. A. & Kouwenhoven, L. P. Quantum supercurrent transistors in carbon nanotubes. *Nature* **439,** 953–956 (2006).
28. Buitelaar, M. R. *et al.* Multiple Andreev reflections in a carbon nanotube quantum dot. *Phys. Rev. Lett.* **91,** 057005 (2003).
29. Blonder, G. E., Tinkham, M. & Klapwijk, T. M. Transition from metallic to tunneling regimes in superconducting micro-constrictions — Excess current, charge imbalance, and super-current conversion. *Phys. Rev. B* **25,** 4515–4532 (1982).
30. Flensberg, K., Hansen, J. B. & Octavio, M. Subharmonic energy-gap structure in superconducting weak links. *Phys. Rev. B* **38,** 8707–8711 (1988).

Acknowledgements

We thank Y.J. Doh and J.U. Free for helpful discussions. M.T. acknowledges support from the National Science Foundation. R.M.W. acknowledges support of this work by DARPA-QuIST and the Nanoscale Science and Engineering Center at Harvard University. C.M.L. acknowledges support of this work by the Defense Advanced Research Projects Agency, Army Research Organization and NSF. Correspondence and requests for materials should be addressed to R.M.W. or C.M.L. Supplementary information accompanies this paper on www.nature.com/naturenanotechnology.

Author contributions

J.X. and A.V. performed the experiments and analysed the data with help from M.T. All the authors discussed the results and co-wrote the manuscript.

Competing financial interests

The authors declare that they have no competing financial interests.